

Electrically and Ionically Conductive Network with High Stretchability Enables High-Performance Micro-Sized Silicon Anode

Gengcong Zhu, Yan Zhu, Anru Guo,* Ke Zhang, Yun Zhou, Tengfei Sun,* and Dong Liu*

Silicon is recognized as a promising anode material for energy-dense lithium-ion batteries due to its high theoretical specific capacity, but encounters great challenges, including huge volume change and unstable interfaces during the cycling process. An electrically and ionically conductive network with high stretchability is reported, prepared from single-walled carbon nanotubes and a polymeric network (PAA-EP), which enables a high-performance micro-sized silicon (μ Si) anode. The PAA-EP network is synthesized through the cross-linking reaction between poly(acrylic acid) and terminal hydroxyl polyethers. Such a binder design combines high strength with exceptional toughness by integrating the stiffness of poly(acrylic acid) with

the pliability of polyethers. The as-prepared μ Si anode with PAA-EP exhibits extremely high initial specific capacity (4030.4 mAh g⁻¹), unprecedented long-term cycle stability (capacity remaining 904 mAh g⁻¹ after 500 cycles at 2.0 A g⁻¹), and superior rate performance (1692 mAh g⁻¹ at 3.0 A g⁻¹). Meanwhile, this network also enables SiO_x anodes with an ultra-high capacity retention of 98.52% at 0.75 A g⁻¹ after 500 cycles (calculated from the 26th cycle), highlighting promising commercial application prospects. This work provides a straightforward yet efficient strategy for stabilizing Si-based anodes, which paves a new way to improve the electrochemical performance of various high-capacity electrode materials.

1. Introduction

Lithium-ion batteries (LIBs) have been widely applied in various fields, including consumer electronics, electric vehicles, and the energy storage field.^[1–5] With the urgent demands of high-energy-density LIBs, the development of high-specific-energy electrode materials has become increasingly significant. Among the extensive anode materials, silicon (Si) is recognized as a promising anode material for energy-dense LIBs due to its much higher theoretical specific capacity (4200 mAh g⁻¹) than currently used graphite (372 mAh g⁻¹).^[6,7] However, the Si-based anodes encounter great challenges for practical application, including huge volume change (300–400%) and unstable interfaces during cycling. This resulted in inevitable fracture or

pulverization of Si particles, electrode structural collapse, and a mechanically unstable solid electrolyte interface (SEI), thereby leading to poor cycle performance, which severely hinders its practical applications in energy-dense batteries.^[8–12] To address these challenges, researchers have developed various strategies, including material structure optimization,^[13–15] the application of functional coatings (e.g., elasticity, electrical conductivity),^[16–18] and the development of novel polymeric binders.^[19]

The binder is a crucial component for connecting active material and conductive agent on the current collector, thereby maintaining electrode structure integrity with high mechanical and adhesive ability.^[20,21] Numerous linear polymers, including polyvinylidene difluoride (PVDF),^[22,23] carboxymethyl cellulose/styrene butadiene rubber (CMC/SBR),^[24,25] sodium alginate (SA),^[26,27] guar gum^[28,29] and poly(acrylic acid) (PAA),^[30–32] have been developed as efficient binders for stable operation of Si-based anodes. However, due to their inherent limitations of weak mechanical property, the cycle performances of Si anodes are still far from for practical application.^[12,33] To address this problem, various binders with a cross-linked network have been investigated for further improving the electrochemical performance of Si-based anodes owing to their high mechanical strain resistance and strong deformation tolerance. Despite the great advances in these binders, the comprehensive electrochemical performance of silicon-based anodes is still not satisfied for practical applications.^[34–37] Therefore, it is desirable to develop advanced binders to meet the performance requirements of silicon anodes for practical commercial application.

Herein, we report an electrically and ionically conductive network (PAA-EP) with high stretchability, which enables a

G. Zhu, Y. Zhu, K. Zhang, Y. Zhou, D. Liu
State Key Laboratory of Organic-Inorganic Composites
College of Chemical Engineering
Beijing University of Chemical Technology
Beijing 100029, P. R. China
E-mail: liudong@mail.buct.edu.cn

A. Guo
Aerospace Research Institute of Materials & Processing Technology
Beijing 100076, P. R. China
E-mail: 200521025@163.com

T. Sun
College of Mechanical and Electrical Engineering
Beijing University of Chemical Technology
Beijing 100029, P. R. China
E-mail: suntengfei@mail.buct.edu.cn

 Supporting information for this article is available on the WWW under <https://doi.org/10.1002/batt.202500471>

high-performance Si-based anode. The PAA-EP network was synthesized via an *in situ* cross-linking reaction between an ion-conductive terminal hydroxyl polyethers (EP) and polyacrylic acid (PAA) during the electrode drying process. More importantly, the single-walled carbon nanotubes (SWCNTs) were uniformly dispersed within the chemically cross-linked PAA-EP network, thereby forming a 3D conductive network (Figure 1a). The PAA-EP binder exhibited outstanding mechanical properties, including high strength, high hardness, large adhesion, and good elasticity, which can effectively alleviate the volume change of the silicon anode during the cycling process. Particularly, the as-prepared μ Si/PAA-EP electrode exhibited extremely high initial specific capacity ($4030.4 \text{ mAh g}^{-1}$), unprecedented long-term cycle stability (capacity remaining 904 mAh g^{-1} after 500 cycles at 2.0 A g^{-1}), and superior rate performance (1692 mAh g^{-1} at 3.0 A g^{-1}). Meanwhile, this conductive network also enabled SiO_x anodes with ultrahigh capacity retention of 98.52% at 0.75 A g^{-1} after 500 cycles (calculated from the 26th cycle), highlighting its promising commercial application prospects. This work provides a simple yet efficient strategy to construct an electrically and ionically conductive network with high stretchability for Si-based anodes, which paves a new way to improve the comprehensive performance of various high-capacity electrode materials.

2. Results and Discussion

2.1. Binder Design and Preparation

To alleviate the large volume change of silicon-based anode during the charging and discharging process, we designed a

network binder with high mechanical properties and high ionic conductivity for achieving stable operation of silicon-based anodes (Figure 1a). Typically, the terminal hydroxyl polyethers (EP) were designed to react with PAA with abundant carboxyl groups for constructing the network with high ionic conductivity owing to the abundant ether bonds of EP.^[38] Importantly, the abundant carboxyl groups of PAA can bond with the hydroxyl groups on the silicon surface to stabilize the interface of the silicon anode.^[39] The combined advantages of EP with PAA endow the network with high stretchability and large ionic conductivity (Figure 1a,b), effectively addressing the issues of poor toughness and low ionic conductivity associated with the PAA binder. The stress concentration of the silicon anode can be more effectively relieved by the PAA-EP network compared to PAA, thus maintaining the integrity of the electrode structure. Additionally, to increase the electronic conductivity of the electrode, the SWCNTs were used as conductive additives because SWCNTs played a key role in enhancing both electrical conductivity and mechanical strength, benefiting to increase the electrochemical performance of micro-sized silicon anodes.^[40] For instance, the micro-sized silicon anodes with SWCNTs additives achieved better cycle stability and rate capability compared to the silicon anodes with multi-walled carbon nanotubes or carbon black additives.^[41,42] More importantly, the SWCNTs were evenly dispersed within the PAA-EP network to form a 3D conductive network. The combined advantages of both PAA-EP network and SWCNTs result in the formation of an electrically and ionically conductive network with high stretchability, enabling stable operation of micro-sized silicon-based anodes. Conversely, the micro-sized silicon anodes based on PAA suffered from the huge volume expansion (Figure 1c), leading to poor electrochemical performance.

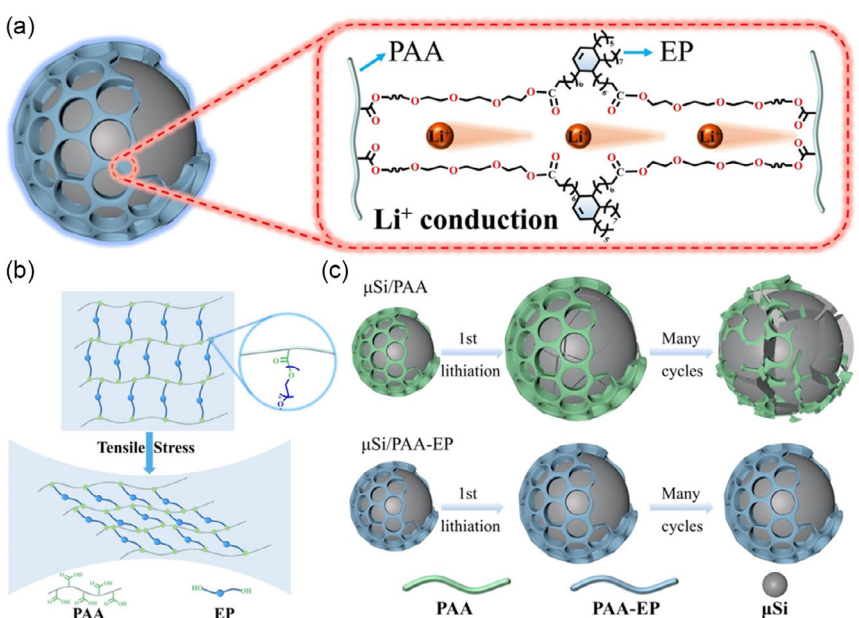


Figure 1. Schematic illustration for a) the formation of PAA-EP network via the reaction between PAA and EP, b) the PAA-EP network during the stretching process, and c) the structure evolution of micro-sized Si electrodes with PAA-EP and PAA, respectively.

The EP was synthesized by the esterification reaction between polyacid (Empol 1016, Figure S1, Supporting Information) and polyethylene glycol at 160 °C for 24 h under an Ar atmosphere, as shown in Figure S2, Supporting Information. The structure of EP was confirmed by its ¹H NMR spectrum in Figure S3, Supporting Information, where the corresponding marked peak can be observed for each hydrogen in the EP. Moreover, the obvious peaks of ester groups at 286.6 eV in high-resolution X-ray photoelectron spectroscopy (XPS) C 1s spectra (Figure S4, Supporting Information) proved the generation of the EP network. To clearly confirm the successful formation of the polymeric network, the chemically cross-linked PAA-EP composite was prepared by the reaction between PAA and EP at 150 °C for 3 h under vacuum conditions, followed by characterized using Fourier transform infrared (FTIR) spectroscopy. FTIR spectrum of PAA-EP in Figure S5, Supporting Information shows that the broad peak intensity of —OH bond associated with terminal hydroxyl groups of EP at 3340 cm⁻¹ obviously decreased because the content of ester bonds increased after the esterification reaction between —COOH groups of PAA and —OH groups of EP, suggesting the formation of chemically cross-linked PAA-EP.^[43,44]

To evaluate the properties of the PAA-EP binder, the μ Si anodes with PAA-EP (μ Si/PAA-EP) were prepared using μ Si powder (Figure S6, Supporting Information), SWCNTs, and PAA-EP (Figure S7, Supporting Information) as active materials, conductive additives, and binder, respectively. The μ Si/PAA-EP anode showed the characteristic peaks corresponding to μ Si and Cu foils, without any additional crystallization by-products (Figure S8, Supporting Information), indicating no structural changes in μ Si particles during the preparation process of μ Si anodes. In the μ Si/PAA-EP electrode, the PAA-EP adsorbs onto SWCNTs through hydrophobic segments of mixed acids, while its hydrophilic moieties (e.g., carboxyl groups, ester linkages, and ether bonds) significantly enhance dispersibility.^[45,46] Besides, ester bonds of PAA-EP interact with SWCNTs via hydrogen bonding or polar adsorption mechanisms.^[47] Based on the interactions between PAA-EP and SWCNTs, the 3D conductive entanglement network was formed during the electrode preparation process, as shown in scanning electron microscope (SEM) image of μ Si/PAA-EP (Figure 2a). Additionally, transmission electron microscope (TEM) image of μ Si/PAA-EP displays that the μ Si particles were bridged by a 3D conductive network (Figure 2b), further

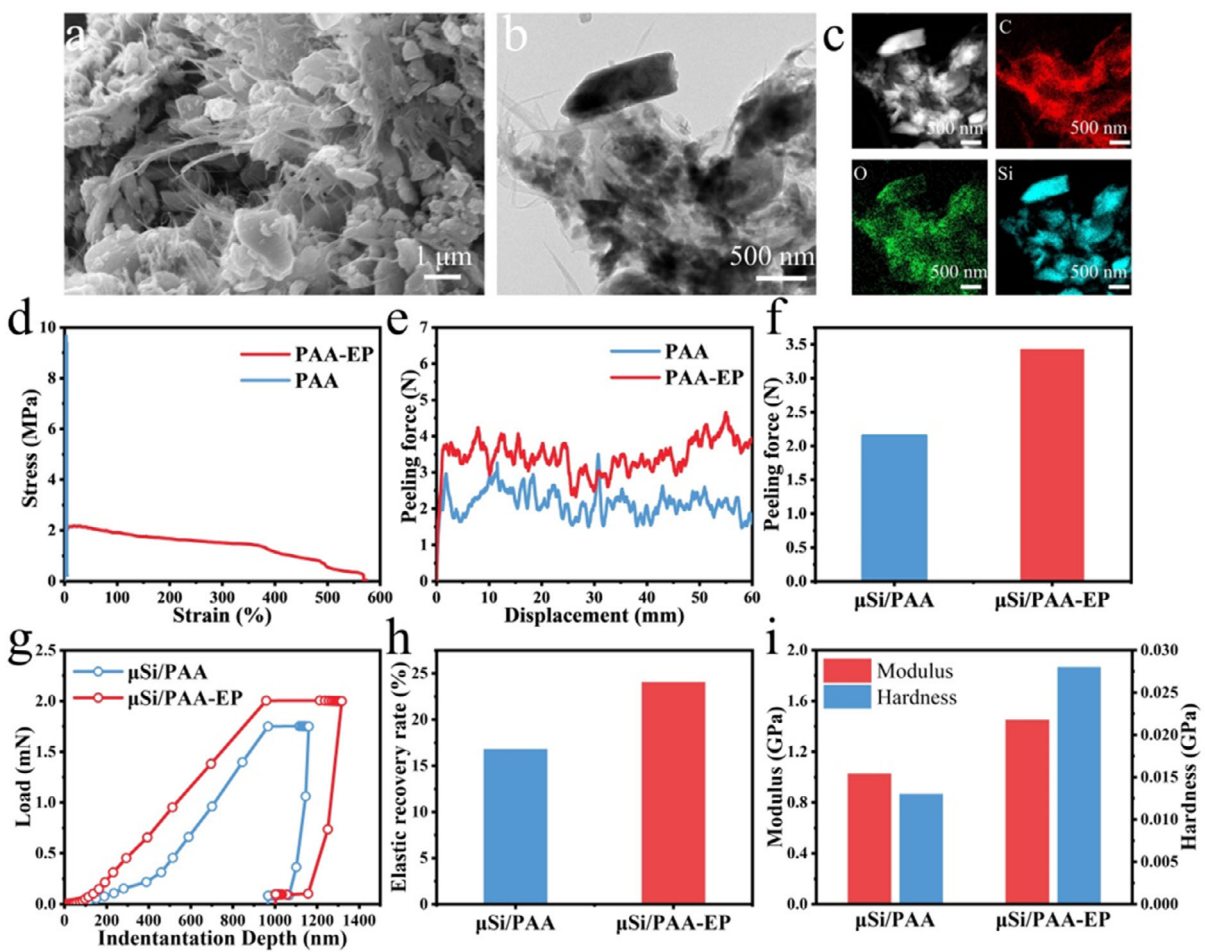


Figure 2. a) Top-viewed SEM image of μ Si/PAA-EP. b) TEM image of μ Si/PAA-EP. c) EDS mapping images of μ Si/PAA-EP. d) Stress–strain curves of PAA-EP and PAA films. e) Peel test curves of μ Si/PAA-EP and μ Si/PAA electrodes. f) Average peel strength of μ Si/PAA-EP and μ Si/PAA electrodes. g) Load–displacement curves of μ Si/PAA-EP and μ Si/PAA electrodes. h) Elastic recovery of μ Si/PAA-EP and μ Si/PAA electrodes. i) Hardness and modulus of μ Si/PAA-EP and μ Si/PAA electrodes.

indicating the presence of a 3D conductive network in the μ Si/PAA-EP electrode. Furthermore, an amorphous SiO_x layer with a thickness of 2.24 nm was observed on the surface of μ Si particles, which possessed lattice edges with a d-spacing of 0.314 nm (Figure S9, Supporting Information), associated with the (111) lattice plane of μ Si particles.^[48] The elemental mapping images in Figure 2c show the uniform distribution of C, O, and Si elements throughout the μ Si/PAA-EP electrode, further revealing the even encapsulation effect of the 3D conductive network on the μ Si particles.

2.2. Mechanical Properties

The introduction of EP can greatly improve the mechanical properties of the PAA binder, as confirmed by the stress-strain curve. As shown in Figure 2d, the PAA-EP spline demonstrates a non-Hookean stress-strain curve with a stress of 2.3 MPa and a strain over 574.8%, indicating that the PAA-EP possessed high strength with good toughness. Figure S10, Supporting Information vividly displays the high stretchability of the PAA-EP network. Contrastly, the PAA spline exhibits obvious brittle behavior with a high stress of 9.8 MPa yet a low strain of only 5.5%. The high stretchability of PAA-EP can be ascribed to the cross-linked polymeric network with high flexibility of the EP chain. Furthermore, the 180° peeling test was performed to evaluate the adhesion of the PAA-EP binder for preparing μ Si electrodes. As shown in Figure 2e,f, the average adhesion of μ Si/PAA-EP (3.43 N) was much higher than that of μ Si/PAA electrode (\approx 2.15 N), suggesting that the PAA-EP network demonstrates superior adhesion to the copper foil collector. The mechanical properties of μ Si/PAA-EP electrodes were further investigated by a nanoindentation test. The load-indentation depth curves in Figure 2g show that the optimal load for the μ Si/PAA-EP electrode (2.002 mN) is significantly higher than that of the μ Si/PAA electrode (1.693 mN) at a controlled indentation depth of about 1000 nm. The indentation depth of μ Si/PAA-EP recovered from 1317.53 to 1001.00 nm after removing the load, resulting in a calculated elastic recovery of 24.02% (Figure 2h), which is significantly higher than that of μ Si/PAA (16.78%). In addition, the μ Si/PAA-EP electrode displayed higher modulus and hardness compared to μ Si/PAA (Figure 2i), indicating a stronger stress tolerance ability. The optimal elastic recovery combined with high deformability was beneficial for alleviating the enormous stress and maintaining electrode integrity during cycling. Furthermore, the PAA-EP with 574.8% strain can efficiently cover the volume change of the μ Si anode (\approx 300%) during cycling.

2.3. Electrochemical Performance

Owing to the excellent mechanical properties of PAA-EP composite, the electrochemical performance of silicon-based anodes with PAA-EP and PAA binders was further evaluated. To optimize the cell performance, μ Si electrodes were prepared using three PAA-EP binders with different mass ratios of PAA to EP (7:3, 8:2, and 9:1), obtaining μ Si/PAA-7-EP, μ Si/PAA-8-EP, and μ Si/PAA-9-EP

electrodes, respectively. Among three μ Si electrodes, the μ Si/PAA-8-EP electrode exhibited the largest initial discharged specific capacity of $4030.4 \text{ mAh g}^{-1}$ and the highest initial Coulomb efficiency (ICE) of 87.99% (Figure S11, Supporting Information), suggesting that the optimal mass ratio of PAA to EP for preparing PAA-EP binder is 8:2. The μ Si/PAA-8-EP electrode also showed the most excellent cycling performance at both current densities of 0.6 and 2.0 A g^{-1} (Figure S12 and S13, Supporting Information). Accordingly, the PAA-8-EP binder was selected for the subsequent study and denoted as PAA-EP. From the above results, we can conclude that the EP chain has a significant effect on the electrochemical performance of μ Si electrode with PAA-EP binder. Therefore, we focused on studying the role of EP in enhancing electrochemical performance, rather than the mass ratio of PAA to EP.

The redox behaviors of μ Si/PAA-EP and μ Si/PAA electrodes during charging and discharging were investigated using cyclic voltammetry (CV) tests. The CV curves of both μ Si/PAA-EP and μ Si/PAA electrodes show similar redox peaks to those observed in most previously reported Si anodes (Figure S14, Supporting Information), suggesting similar redox behaviors.^[49,50] Interestingly, the μ Si/PAA-EP electrode exhibited higher initial specific capacity ($4030.4 \text{ mAh g}^{-1}$) and ICE (87.99%) compared to the μ Si/PAA electrode (specific capacity: $3118.1 \text{ mAh g}^{-1}$, ICE: 86.36%), as shown in Figure 3a,b. Furthermore, the μ Si/PAA-EP electrode also achieved superior cycling performance than that of the μ Si/PAA electrode at different current densities (Figure 3c,d, S15 and S16, Supporting Information). Figure 3c shows that the capacity retention of the μ Si/PAA-EP electrode (82.82%, calculated from the 20th cycle) was obviously higher than that of the μ Si/PAA electrode (48.87%) after 100 cycles at a current density of 0.6 A g^{-1} . Additionally, after 500 cycles at a high current density of 2.0 A g^{-1} , the μ Si/PAA-EP electrode retained a high capacity of 904 mAh g^{-1} , whereas the μ Si/PAA electrode exhibited a low capacity of only 359.2 mAh g^{-1} (Figure 3d), suggesting excellent long-term stability of the μ Si/PAA-EP electrode. Figure 3e displays the excellent rate performance of μ Si/PAA-EP electrode at different current densities, as exemplified by the high discharge specific capacity of 1692 mAh g^{-1} even at a high current density of 3.0 A g^{-1} . When the current density returned to 0.6 A g^{-1} , the capacity of the μ Si/PAA-EP electrode recovered to $3120.1 \text{ mAh g}^{-1}$, indicating its good recovery ability. In addition, exceptional cycling stability and rate performance of μ Si/PAA-EP make it possible to explore the potential of the μ Si anodes with high mass loading, which is also significant to develop next-generation high-energy-density LIBs. As shown in Figure 3f, the μ Si/PAA-EP electrode with a μ Si mass loading of 2.159 mg cm^{-2} exhibited a high areal capacity of $5.555 \text{ mAh cm}^{-2}$ at 0.6 A g^{-1} and maintained an area capacity of $3.788 \text{ mAh cm}^{-2}$ after 50 cycles, corresponding to a capacity retention of about 68.25%. Furthermore, the evolving trend of areal capacity with increasing current density at high mass loading was shown in Figure 3g. Apparently, PAA-EP enabled the μ Si anode to achieve a high and stable areal capacity at moderate current densities ($<3.2 \text{ mA cm}^{-2}$), even at a high loading of 5.326 mg cm^{-2} . This excellent electrochemical performance can

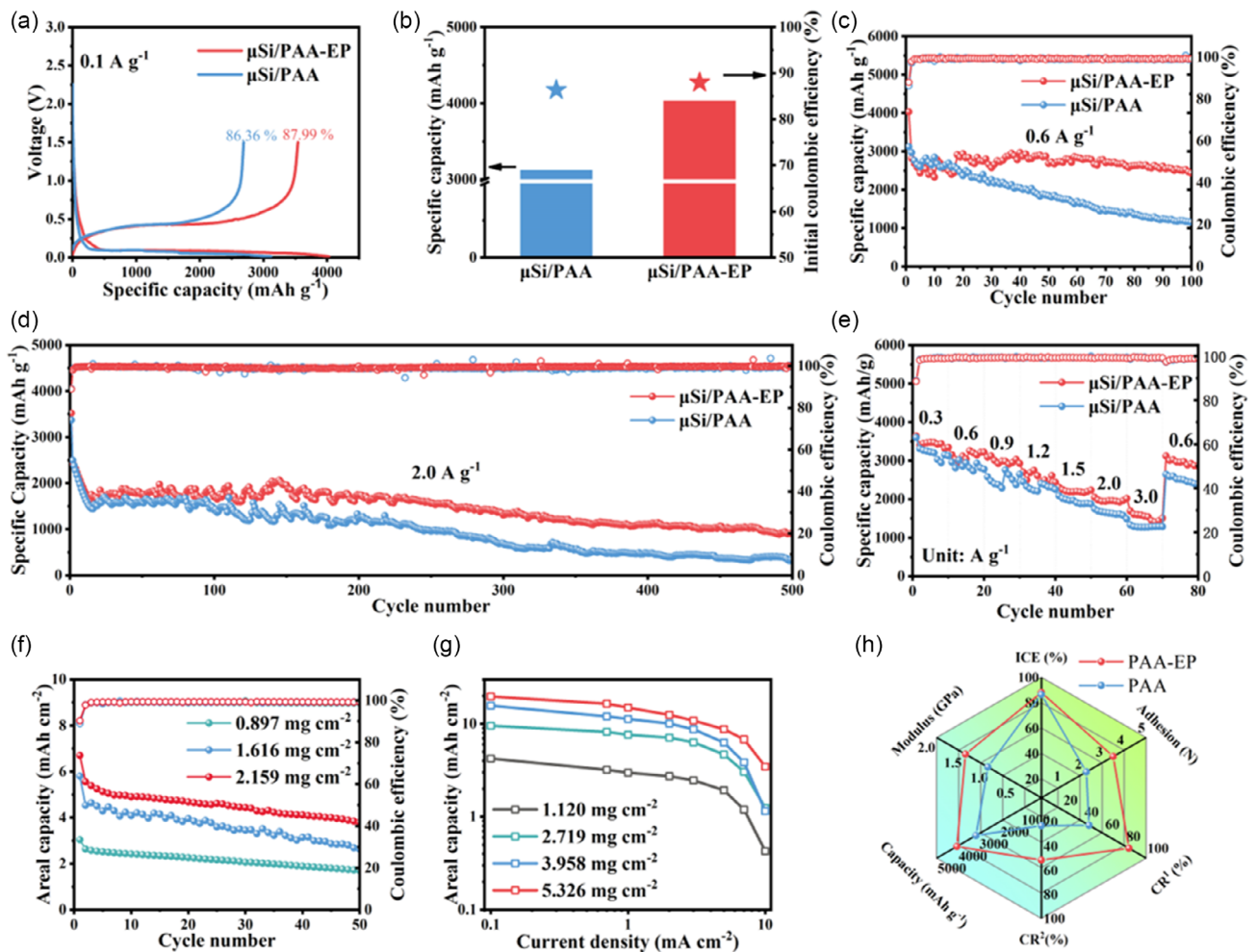


Figure 3. a) Initial discharge and charge curves of $\mu\text{Si}/\text{PAA}$ and $\mu\text{Si}/\text{PAA-EP}$ electrodes. b) ICE of $\mu\text{Si}/\text{PAA}$ and $\mu\text{Si}/\text{PAA-EP}$ electrodes. c) Cycling performance of $\mu\text{Si}/\text{PAA}$ and $\mu\text{Si}/\text{PAA-EP}$ electrodes at 0.6 A g^{-1} . d) Cycling performance of $\mu\text{Si}/\text{PAA}$ and $\mu\text{Si}/\text{PAA-EP}$ electrodes at 2.0 A g^{-1} . e) Rate performance of $\mu\text{Si}/\text{PAA}$ and $\mu\text{Si}/\text{PAA-EP}$ electrodes. f) Cycling performance of $\mu\text{Si}/\text{PAA-EP}$ with varying μSi mass loading at 0.6 A g^{-1} . g) The effect of current density and mass loading on the areal capacity of $\mu\text{Si}/\text{PAA-EP}$ electrodes. h) Radar chart comparing the ICE, adhesion strength, modulus, capacity, and capacity retention rate (CR1 at 0.6 A g^{-1} , CR2 at 2.0 A g^{-1}) between $\mu\text{Si}/\text{PAA}$ and $\mu\text{Si}/\text{PAA-EP}$ electrodes.

be attributed to the high mechanical properties (Figure 2) and superior electron/ionic conductivity delivered by the PAA-EP network, as discussed below.^[51] The superior overall performance of the $\mu\text{Si}/\text{PAA-EP}$ electrode compared to the $\mu\text{Si}/\text{PAA}$ electrode (Figure 3h) highlights the excellent suitability of the PAA-EP network for stable operation of the μSi anode. Furthermore, the PAA-EP binder enables Si-based anodes with an impressive high specific capacity of 904 mAh g^{-1} at 2.0 A g^{-1} after long-term 500 cycles, highly competitive with most previously reported advanced binders for Si-based LIBs (Table S1 and Figure S17, Supporting Information).

Apart from μSi anodes, the electrochemical performance of commercial SiO_x powders (Figure S18, Supporting Information) was also investigated to further assess the universality of PAA-EP binders for stabilizing different high-capacity electrodes. The same preparation method used for the μSi electrode was employed to fabricate the $\text{SiO}_x/\text{PAA-EP}$ electrode. The constant current charge/discharge curves in Figure S19, Supporting

Information illustrate that the $\text{SiO}_x/\text{PAA-EP}$ electrode delivered markedly higher initial specific capacity ($2523.9 \text{ mAh g}^{-1}$) and ICE (63.46%) than that of the SiO_x/PAA (specific capacity: $2176.3 \text{ mAh g}^{-1}$, ICE: 52.69%) at 0.1 C ($1 \text{ C} = 2600 \text{ mAh g}^{-1}$). Moreover, the $\text{SiO}_x/\text{PAA-EP}$ electrode achieved obviously better cycle stability at 0.3 A g^{-1} and rate performance than that of SiO_x/PAA (Figure S20 and S21, Supporting Information). Remarkably, the $\text{SiO}_x/\text{PAA-EP}$ electrode achieved a capacity retention of 98.52% even at a current density of 0.75 A g^{-1} (0.5 C) after 500 cycles (calculated from the 26th cycle), while the SiO_x/PAA electrode retained a capacity retention of only 55.94% (Figure S22, Supporting Information). The poor cycle stability of the SiO_x/PAA electrode is attributed to the inability of PAA to provide sufficient toughness to withstand the significant stresses generated by the volume change of SiO_x .^[52] The excellent electrochemical performance of $\text{SiO}_x/\text{PAA-EP}$ electrodes highlights the universal of PAA-EP binder for stabilizing high-capacity anodes.

2.4. Reaction Kinetics

To gain a deep understanding of the effect of different binders on the kinetic behaviors of the μ Si anode, CV tests were conducted at varying scanning rates from 0.2 to 1.2 mV s⁻¹, along with galvanostatic intermittent titration technique (GITT) and electrochemical impedance spectroscopy (EIS) tests on μ Si/PAA and μ Si/PAA-EP electrodes. According to the CV curves of μ Si/PAA and μ Si/PAA-EP electrodes in Figure 4a,b, a linear relationship between the peak current and the square root of scanning rates was obtained using the Randles-Sevcik Equation (Figure 4c,d). The slope of the linearly fitted line represents the apparent Li⁺ diffusion coefficient (D_{Li^+}). The D_{Li^+} values of μ Si/PAA and μ Si/PAA-EP electrodes during lithiation were calculated as 1.48×10^{-11} and 5.85×10^{-10} cm²s⁻¹, whereas the values during delithiation were 1.97×10^{-11} and 6.16×10^{-10} cm²s⁻¹,

respectively. Obviously, the μ Si/PAA-EP electrode possessed a higher D_{Li^+} compared to the μ Si/PAA electrode during both the charging and discharging processes, indicating a faster Li⁺ diffusion rate for the μ Si/PAA-EP electrode. In addition, the D_{Li^+} values of two electrodes during the charging and discharging process were further evaluated by GITT, as reflected by the Li⁺ diffusion rate after 20 cycles (Figure S23, Supporting Information). As shown in Figure 4g,h, the calculated D_{Li^+} of μ Si/PAA-EP after activation was significantly higher than that of μ Si/PAA electrode during lithiation and delithiation according to Fick's second law.^[54,55] To provide the direct evidence for the high ionic conductivity of the binder, the binder film was prepared and measured by EIS. The fitted EIS spectra in Figure S24, Supporting Information showed that the PAA-EP film possessed an ionic conductivity of 25.8 μ S cm⁻¹, which is obviously larger than that of PAA (11.6 μ S cm⁻¹), demonstrating the role of PAA-EP binder

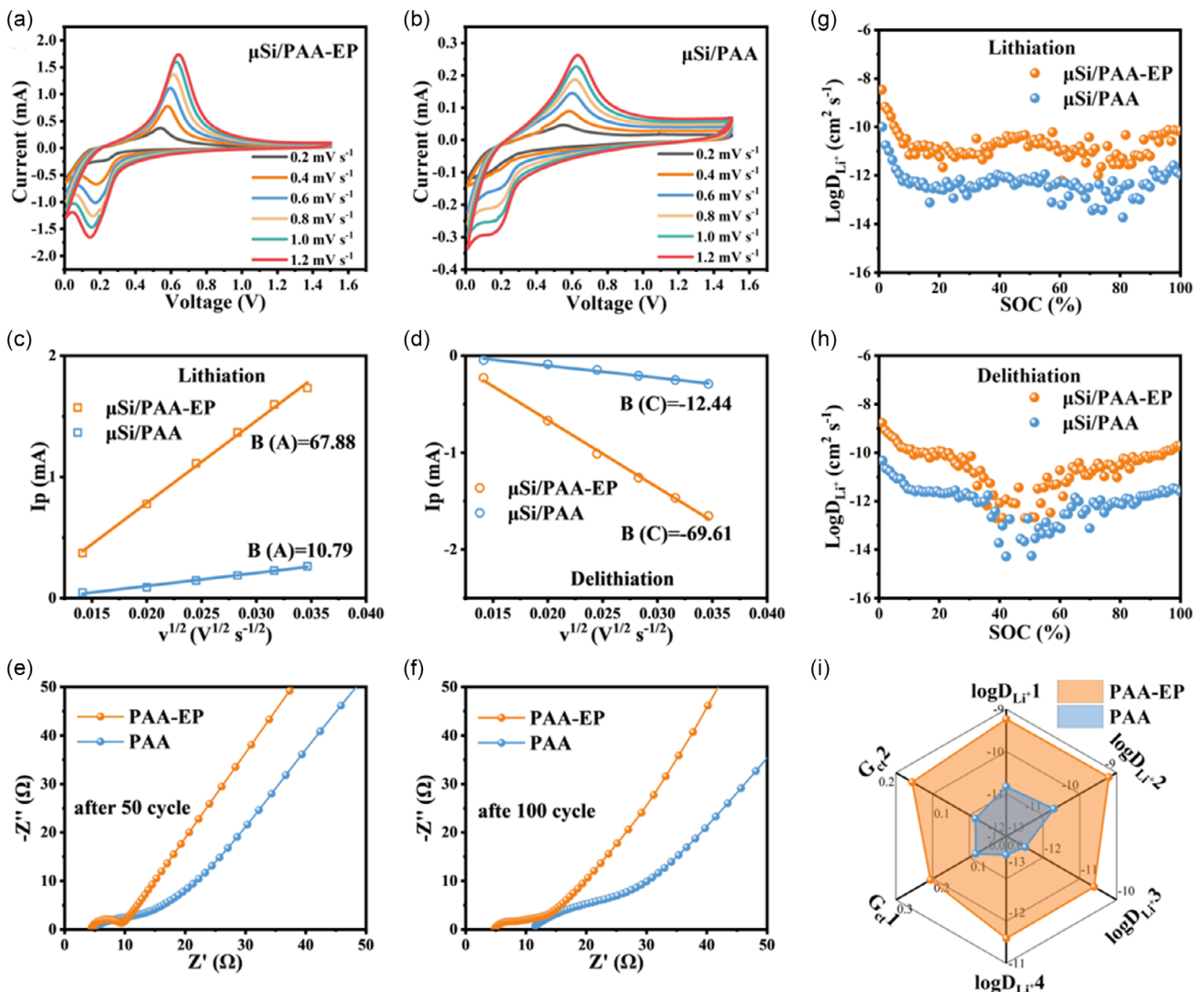


Figure 4. CV curves at different scanning rates from 0.2 to 1.2 mV s⁻¹ for a) μ Si/PAA-EP and b) μ Si/PAA. The relationship of peak current versus the square root of the scanning rates during c) lithiation and d) delithiation process. The fitted EIS spectra of μ Si/PAA-EP and μ Si/PAA after e) 50 and f) 100 cycles. The calculated D_{Li^+} of as-prepared μ Si anodes after 20 cycles during g) lithiation and h) delithiation process. i) Radar chart comparing the apparent Li⁺ diffusion coefficient ($\log D_{Li^+} 1$ for lithiation, $\log D_{Li^+} 2$ for delithiation), D_{Li^+} during charging and discharging ($\log D_{Li^+} 3$ for lithiation, $\log D_{Li^+} 4$ for delithiation), reciprocal of the charge transfer impedance R_{ct} (G_{ct1} after 50 cycles, G_{ct2} after 100 cycles) of μ Si/PAA and μ Si/PAA-EP electrodes.

in facilitating ionic transport for the electrode. This result indicates that the PAA-EP binder enabled more efficient and faster reaction kinetics for the Si anode compared to the PAA binder, in accordance with the results from CV tests (Figure 4c,d).

To further study the electrochemical kinetics of different electrodes during cycling, EIS tests and corresponding impedance simulations were carried out after 50 and 100 cycles. The fitted EIS spectra in Figure 4e,f showed a smaller change of both SEI resistance (R_{SEI} , from 1.31 to 2.21 Ω) and charge transfer resistance (R_{ct} , from 4.85 to 5.86 Ω) for μ Si/PAA-EP from 50 to 100 cycles compared to R_{SEI} (from 4.11 to 10.80 Ω) and R_{ct} (from 12.01 to 17.92 Ω) for μ Si/PAA electrode, suggesting a more stable electrode structure and faster charge transfer ability of μ Si/PAA-EP electrode. Consequently, the μ Si/PAA-EP electrode exhibits larger D_{Li^+} and smaller interface resistance as well as charge transfer

resistance, indicating that the PAA-EP network facilitated the formation of Li^+ transport channel, and accelerated reaction kinetics of Si-based anodes. Benefiting from a high cross-linking network accompanied by excellent mechanical properties, the large volume expansion of Si-based anodes during cycling would be effectively suppressed, thus improving cycle stability. Combined with the mechanical properties with rapid Li^+ transport ability in the PAA-EP network, the μ Si/PAA-EP electrode illustrated superior electrochemical performance than that of μ Si/PAA.

2.5. Structural Characterization and Surface Composition Analysis

SEM analysis was carried out to further clearly reveal the important role of the high mechanical properties of the PAA-EP network binder in maintaining the integrity of the electrode

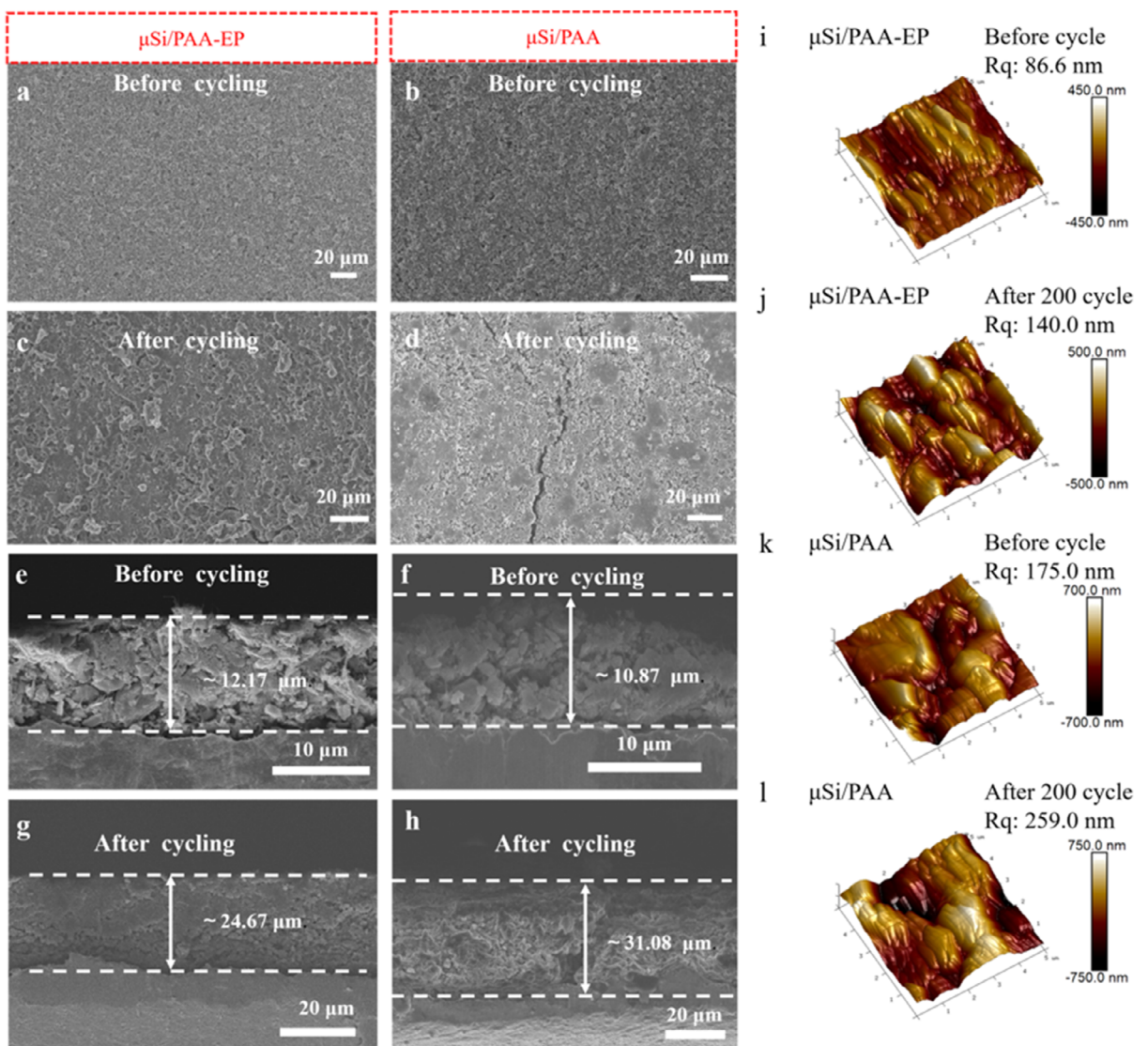


Figure 5. Top-viewed SEM images of a) μ Si/PAA-EP and b) μ Si/PAA electrodes before cycling. Top-viewed SEM images of c) μ Si/PAA-EP and d) μ Si/PAA electrodes after 200 cycles at 2 A g^{-1} . Cross-sectional SEM images of e) μ Si/PAA-EP and f) μ Si/PAA electrodes before cycling. Cross-sectional SEM images of g) μ Si/PAA-EP and h) μ Si/PAA electrodes after 200 cycles at 2 A g^{-1} . AFM images of μ Si/PAA-EP electrode i) before and j) after 200 cycles at 2 A g^{-1} . AFM images of μ Si/PAA electrode k) before and l) after 200 cycles at 2 A g^{-1} .

structure through preventing the volume expansion of μ Si. As shown in Figure 5a,b, good integrity and smooth surface morphology of μ Si/PAA-EP and μ Si/PAA electrodes were observed before cycling. However, the μ Si/PAA-EP electrode showed slight cracking and damage after 200 cycles at a current density of 2 A g^{-1} (Figure 5c), while μ Si/PAA exhibited a severe cracking and detachment of the active material due to undesirable stress changes in μ Si/PAA electrode (Figure 5d). The thickness changes

of the μ Si electrodes can be directly demonstrated by the cross-sectional SEM images (Figure 5e–h), which illustrate that the PAA-EP network plays a great role in inhibiting the volume expansion of μ Si. The original thicknesses of the μ Si/PAA-EP and μ Si/PAA electrodes are 12.17 and $10.87 \mu\text{m}$, respectively. After cycling, the thickness of μ Si/PAA-EP electrode increased to $24.67 \mu\text{m}$ with a volume expansion rate of 102.7% , while the μ Si/PAA electrode displayed a volume expansion rate of 185.9% with the thickness

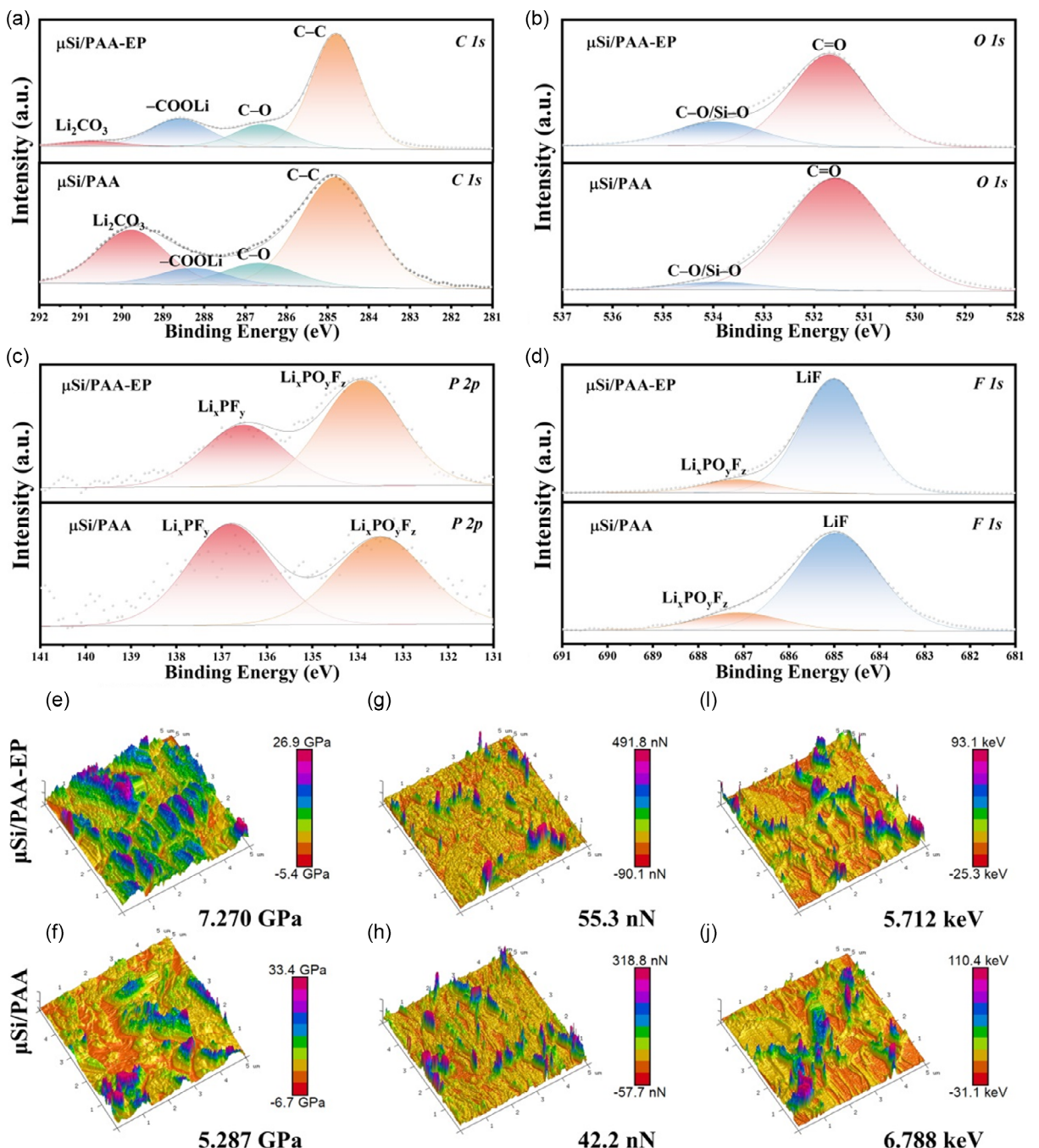


Figure 6. High-resolution XPS spectra of μ Si/PAA-EP and μ Si/PAA electrodes after 200 cycles: a) C 1s, b) O 1s, c) P 2p, d) F 1s. DMT modulus mappings of e) μ Si/PAA-EP and f) μ Si/PAA electrodes. Adhesion mappings of g) μ Si/PAA-EP and h) μ Si/PAA electrodes. Energy dissipation images of i) μ Si/PAA-EP and j) μ Si/PAA electrodes.

increased to 31.08 μm . Obviously, PAA-EP showed a significant advantage in mitigating the volume expansion of μSi compared with PAA.

The evolution of electrode surface roughness was measured by atomic force microscopy (AFM) during cycling. The 3D surface morphology of $\mu\text{Si}/\text{PAA-EP}$ and $\mu\text{Si}/\text{PAA}$ electrodes was shown in Figure 5i–l. Before cycling, the surface roughness (R_q) values of the $\mu\text{Si}/\text{PAA-EP}$ and $\mu\text{Si}/\text{PAA}$ electrodes were 86.6 and 175.0 nm, respectively. The 3D surface roughness of the $\mu\text{Si}/\text{PAA-EP}$ electrode slightly increased to 140.0 nm (Figure 5j) after 200 cycles at 2 A g $^{-1}$, while the surface roughness of $\mu\text{Si}/\text{PAA}$ electrode significantly increased to 259.0 nm (Figure 5l). Above results suggest that the surface roughness change of $\mu\text{Si}/\text{PAA-EP}$ before and after cycling is obviously lower than that of $\mu\text{Si}/\text{PAA}$, further confirming that the PAA-EP network enabled a stable electrode structure of the μSi anode by relieving the unfavorable stress during cycling. These results indicated that PAA-EP was more suitable for mitigating the huge volume expansion of μSi and reducing the fragmented area of the electrode, thus maintaining the integrity of the electrode and thus improving the cycling performance.

Furthermore, the surface composition analysis of the μSi electrodes after 200 cycles was conducted through XPS. The high-resolution XPS C 1s spectra (Figure 6a) showed larger contents of carbon-containing species associated with electrolyte decomposition products (e.g., alkyl carbonate, alkyl carboxylates, and Li_2CO_3)^[56,57] on the $\mu\text{Si}/\text{PAA}$ electrode compared to the $\mu\text{Si}/\text{PAA-EP}$ electrode. The prominent peaks of $\text{Li}_x\text{PO}_y\text{F}_z$ and Li_xPF_y were detected from the $\mu\text{Si}/\text{PAA}$ electrode (Figure 6c,d), attributing to the uncontrollable decomposition of carbonate-based electrolytes and lithium salt in the PAA electrode than the $\mu\text{Si}/\text{PAA-EP}$ electrode.^[58,59] As the Si surface is newly exposed due to the breakdown of the SEI layers, the electrolyte could decompose, leading to the regeneration of $\text{Li}_x\text{PO}_y\text{F}_z$. Additionally, the $\mu\text{Si}/\text{PAA-EP}$ electrode exhibits a dominant LiF peak, which is usually formed on silicon particles surface (Figure 6d, Table S2, Supporting Information). Considering the fractions of these inorganic components, the $\mu\text{Si}/\text{PAA-EP}$ electrode should possess a more stable and homogeneous SEI film than the $\mu\text{Si}/\text{PAA}$ electrode. Therefore, all the above results proved that the PAA-EP binder is favorable to construct a uniform and stable SEI film, which is desirable to achieve long-term cycling stability of Si-based anodes.

2.6. Stress Distribution Ability

In view of the superior electrochemical performance of $\mu\text{Si}/\text{PAA-EP}$, AFM analysis with the Peak-Force quantitative nanomechanical model (QNM) was applied to further investigate the stress distribution ability of the network binder. Typically, the modulus of μSi electrodes obtained by the Derjaguin–Muller–Toporov model is denoted as the DMT modulus.^[60,61] The $\mu\text{Si}/\text{PAA-EP}$ electrode exhibited much higher DMT modulus (7.270 GPa) than that of the $\mu\text{Si}/\text{PAA}$ electrode (5.287 GPa), indicating better stress tolerability of the PAA-EP network (Figure 6e,f). Additionally,

the average adhesive force of the $\mu\text{Si}/\text{PAA-EP}$ electrode (55.3 nN, Figure 6g) was higher than that of the $\mu\text{Si}/\text{PAA}$ electrode (42.2 nN, Figure 6h), coinciding with the results in Figure 2e,f. The high modulus and strong adhesion jointly contribute to the excellent mechanical properties of the $\mu\text{Si}/\text{PAA-EP}$ electrode. Furthermore, the $\mu\text{Si}/\text{PAA-EP}$ electrode showed smaller energy dissipation of 5.712 keV (Figure 6i) compared to the $\mu\text{Si}/\text{PAA}$ electrode (6.788 keV, Figure 6j), suggesting less irreversible stress variation of the $\mu\text{Si}/\text{PAA-EP}$ electrode yet high stress distribution ability of the PAA-EP network.^[62,63] These results further highlighted less irreversible deformation and crack formation on the $\mu\text{Si}/\text{PAA-EP}$ electrode during cycling, indicating better electrode integrity of $\mu\text{Si}/\text{PAA-EP}$ due to the high stress distribution ability of the PAA-EP network, ascribing to its highly cross-linked network structure.

3. Conclusion

In summary, we report an electrically and ionically conductive network with high stretchability for stable operation of micro-sized silicon-based anode, prepared from the PAA-EP network and SWCNTs. The resulting PAA-EP network exhibited outstanding mechanical properties, including high strength, large hardness, strong adhesion, and high elasticity, which effectively suppresses the volume change of the silicon anode during the charging and discharging process. As a result, the as-prepared $\mu\text{Si}/\text{PAA-EP}$ electrode exhibited extremely high specific capacity, unprecedented long-term cycle stability, and superior rate performance. It's noteworthy that this network also enabled SiO_x anodes with ultrahigh capacity retention of 98.52% after 500 cycles at 0.75 A g $^{-1}$ for commercial applications. This work presents a simple yet efficient strategy to prepare an effective network binder for high-capacity Si-based anodes, which holds promise for inspiring the design of next-generation functional binders to ensure the stable operation of various high-capacity electrode materials.

4. Experimental Section

Detailed experimental procedures can be found in the Supporting Information.

Supporting Information

Supporting information for this article is available on the WWW under <https://doi.org/10.1002/batt.202500471>

Acknowledgements

This work was supported by the Fundamental Research Funds for the Central Universities (buctrc202007).

Conflict of Interest

The authors declare no conflict of interest.

Author Contributions

Gengcong Zhu: data curation (equal); formal analysis lead; investigation (equal); writing—original draft (supporting). **Yan Zhu:** investigation (equal); writing—original draft (lead). **Anru Guo:** funding acquisition (equal); investigation (supporting); supervision (supporting); writing—review and editing (equal). **Ke Zhang:** formal analysis (supporting); investigation (supporting). **Yun Zhou:** data curation (supporting); formal analysis (supporting). **Tengfei Sun:** funding acquisition (equal); supervision (supporting); writing—review and editing (equal). **Dong Liu:** funding acquisition (equal); project administration (lead); writing review and editing (equal). **Gengcong Zhu and Yan Zhu** contributed equally to this work.

Data Availability Statement

The data that support the findings of this study are available from the corresponding author upon reasonable request.

Keywords: electrically and ionically conductive networks • high-capacity silicon anodes • high stretchability • lithium-ion batteries • volumetric changes

- [1] C. Sun, H. Zhang, P. Mu, G. Wang, C. Luo, X. Zhang, C. Gao, X. Zhou, G. Cui, *ACS Nano* **2024**, *18*, 2475.
- [2] X. Zeng, M. Li, D. A. El-Hady, W. Alshitarai, A. S. Al-Bogami, J. Lu, K. Amine, *Adv. Energy Mater.* **2019**, *9*, 1900161.
- [3] H. Jia, X. Li, J. Song, X. Zhang, L. Luo, Y. He, B. Li, Y. Cai, S. Hu, X. Xiao, C. Wang, K. M. Rosso, R. Yi, R. Patel, J. G. Zhang, *Nat. Commun.* **2020**, *11*, 1474.
- [4] H. Sun, G. Xin, T. Hu, M. Yu, D. Shao, X. Sun, J. Lian, *Nat. Commun.* **2014**, *5*, 4526.
- [5] H. Jia, J. Zheng, J. Song, L. Luo, R. Yi, L. Estevez, W. Zhao, R. Patel, X. Li, J. G. Zhang, *Nano Energy* **2018**, *50*, 589.
- [6] Y. Cui, *Nat. Energy* **2021**, *6*, 995.
- [7] D. Ma, Z. Cao, A. Hu, *Nano-Micro Lett.* **2014**, *6*, 347.
- [8] Y. J. Gao, C. H. Cui, Z. K. Huang, G. Y. Pan, Y. F. Gu, Y. N. Yang, F. Bai, Z. Sun, T. Zhang, *Angew. Chem., Int. Ed.* **2024**, *63*, e202404637.
- [9] Q. Li, J. Ruan, S. Weng, X. Zhang, J. Hu, H. Li, D. Sun, X. Wang, F. Fang, F. Wang, *Angew. Chem., Int. Ed.* **2023**, *62*, e202310297.
- [10] M. Khan, S. Yan, M. Ali, F. Mahmood, Y. Zheng, G. Li, J. Liu, X. Song, Y. Wang, *Nano-Micro Lett.* **2024**, *16*, 179.
- [11] Y. Zhou, Y. Yang, G. Hou, D. Yi, B. Zhou, S. Chen, T. D. Lam, F. Yuan, D. Golberg, X. Wang, *Nano Energy* **2020**, *70*, 104568.
- [12] Z. Hu, R. Zhao, J. Yang, C. Wu, Y. Bai, *Energy Storage Mater.* **2023**, *59*, 102776.
- [13] L. Sun, L. Wang, Y. Liu, H. Wang, Z. Jin, *J. Mater. Chem. A* **2025**, *13*, 14346.
- [14] L. Sun, Y. Liu, L. Wang, Z. Chen, Z. Jin, *Nano Res.* **2024**, *17*, 9737.
- [15] X. Jiang, L. Sun, Y. Lu, H. Wang, J. Shi, L. Yang, L. Zhang, R. Lv, Z. Jin, *J. Power Sources* **2024**, *602*, 234331.
- [16] J. Ji, J. Jeong, S. Hong, Y. Lee, D. Kim, W. B. Kim, *Batteries Supercaps* **2025**, 2500037, <https://doi/10.1002/batt.202500037>.
- [17] L. Li, Q. Shi, Z. Wang, C. Zhang, J. Wang, J. Zhang, X. Liu, A. Bachmatiuk, R. Yang, Y. Shen, M. H. Rümmeli, *Batteries Supercaps* **2025**, 2500185, <https://doi/10.1002/batt.202500185>.
- [18] L. Sun, X. Wang, Y. Liu, H. Xu, H. Wang, Y. Lu, Z. Jin, *ACS Appl. Mater. Interfaces* **2024**, *16*, 52349.
- [19] D. Lusztig, S. Luski, N. Shpigel, N. Vangapally, D. Aurbach, *Batteries Supercaps* **2024**, *7*, e202400255.
- [20] Y. M. Zhao, F. S. Yue, S. C. Li, Y. Zhang, Z. R. Tian, Q. Xu, Y. G. Guo, *InfoMat* **2021**, *3*, 460.
- [21] C. C. Wu, C. C. Li, *ACS Sustainable Chem. Eng.* **2020**, *8*, 6868.
- [22] W. Huang, W. Wang, Y. Wang, Q. Qu, C. Jin, H. Zheng, *J. Mater. Chem. A* **2021**, *9*, 1541.
- [23] X. Zhao, S. Niketic, C. H. Yim, J. Zhou, J. Wang, Y. Abu-Lebdeh, *ACS Omega* **2018**, *3*, 11684.
- [24] J. Li, R. B. Lewis, J. R. Dahn, *Electrochim. Solid State Lett.* **2007**, *10*, A17.
- [25] B. Gendensuren, E. S. Oh, *J. Power Sources* **2018**, *384*, 379.
- [26] I. Kovalenko, B. Zdyrko, A. Magasinski, B. Hertzberg, Z. Milicev, R. Burtovy, I. Luzinov, G. Yushin, *Science* **2011**, *334*, 75.
- [27] S. Choi, T. W. Kwon, A. Coskun, J. W. Choi, *Science* **2017**, *357*, 279.
- [28] S. Li, Y. J. Zhong, Y. Song, X. D. Guolonus, *2021*, *27*, 1829.
- [29] M. Q. Jia, X. Qin, X. H. Zhang, J. F. Wang, S. S. Liu, L. Wang, Z. Zhang, N. Q. Miao, G. S. Jiang, Y. Y. Li, H. Wang, *J. Power Sources* **2023**, *561*, 232759.
- [30] B. Hu, I. A. Shkrob, S. Zhang, L. Zhang, J. Zhang, Y. Li, C. Liao, Z. Zhang, W. Lu, L. Zhang, *J. Power. Sources* **2018**, *378*, 671.
- [31] P. Pritesh, M. Sina, A. Banerjee, X. F. Wang, M. S. D'Souza, J. M. Doux, E. A. Wu, O. Y. Trieu, Y. B. Gong, Q. Zhou, K. Snyder, M. Y. Shirley, *Chem. Mater.* **2019**, *31*, 2535.
- [32] C. Li, T. Shi, H. Yoshitake, H. Wang, *J. Mater. Chem. A* **2016**, *43*, 16982.
- [33] Y. M. Zhao, F. S. Yue, S. C. Li, Y. Zhang, Z. R. Tian, Q. Xu, S. Xin, Y. G. Guo, *InfoMat* **2021**, *3*, 460.
- [34] R. Guo, S. Zhang, H. Ying, W. Yang, J. Wang, W. Han, *ChemSusChem* **2019**, *12*, 4838.
- [35] P. F. Cao, G. Yang, B. Li, Y. Zhang, S. Zhao, S. Zhang, A. Erwin, Z. Zhang, A. P. Sokolov, J. Nanda, T. Saito, *ACS Energy Lett.* **2019**, *4*, 1171.
- [36] S. N. S. Hapuarachchi, K. C. Wasalathilake, J. Y. Nerkar, E. Jaatinen, A. P. O'Mullane, C. Yan, *ACS Sustainable Chem. Eng.* **2020**, *8*, 9857.
- [37] H. Liu, T. Chen, Z. Xu, Z. Liu, J. Yang, J. Chen, *ACS Appl. Mater. Interfaces* **2020**, *12*, 54842.
- [38] W. Zeng, L. Wang, X. Peng, T. Liu, Y. Jiang, F. Qin, L. Hu, P. K. Chu, K. Huo, Y. Zhou, *Adv. Energy Mater.* **2018**, *8*, 1702314.
- [39] L. Hu, X. Zhang, P. Zhao, H. Fan, Z. Zhang, J. Deng, G. Ungar, J. Song, *Adv. Mater.* **2021**, *33*, 2104416.
- [40] S. H. Park, P. J. King, R. Tian, C. S. Boland, J. Coelho, C. Zhang, P. McBean, N. McEvoy, M. P. Kremer, D. Daly, J. N. Coleman, V. Nicolosi, *Nat. Energy* **2019**, *4*, 560.
- [41] B. Zhang, D. Liu, H. Xie, D. Wang, C. Hu, L. Dai, *J. Power Sources* **2022**, *539*, 231591.
- [42] B. Zhang, Z. Li, H. Xie, Y. Dong, P. Xu, D. Wang, A. Guo, D. Liu, *J. Power Sources* **2023**, *556*, 232495.
- [43] J. X. Xue, S. X. Jia, T. Q. Xiang, J. J. Zhou, L. Li, *ACS Appl. Mater. Interfaces* **2024**, *16*, 38458.
- [44] B. Koo, H. Kim, Y. Cho, K. T. Lee, N. S. Choi, J. Cho, *Angew. Chem., Int. Ed.* **2012**, *51*, 8892.
- [45] W. Wenseleers, I. I. Vlasov, E. Goovaerts, E. D. Obraztsova, A. S. Lobach, A. Bouwen, *Adv. Funct. Mater.* **2004**, *14*, 1105.
- [46] R. Bandyopadhyaya, E. Nativ-Roth, O. Regev, R. Yerushalmi-Rozen, *Nano Lett.* **2002**, *2*, 25.
- [47] X. Xie, Y. Mai, X. Zhou, *Mater. Sci. Eng. R* **2005**, *49*, 89.
- [48] B. Zhang, Y. Dong, J. Han, Y. Zhen, C. Hu, D. Liu, *Adv. Mater.* **2023**, *35*, 2301320.
- [49] Y. Dong, B. Zhang, F. Zhao, F. Gao, D. Liu, *Small* **2023**, *19*, 2206858.
- [50] F. Li, Y. Xu, L. Chen, J. Xie, L. Jiang, Z. Liang, G. Zang, Z. Zhang, *Chem. Eng. J.* **2024**, *499*, 156644.
- [51] X. Jiao, J. Yin, X. Xu, J. Wang, Y. Liu, *Adv. Funct. Mater.* **2021**, *31*, 2005699.
- [52] D. H. Weng, L. Z. Wu, Z. F. He, D. Y. Zhu, Y. Li, B. Ma, Q. Y. Liu, L. H. Chen, Z. Lin, X. Q. Qiu, *Chem. Eng. J.* **2024**, *499*, 156360.
- [53] T. W. Kwon, Y. K. Jeong, E. Deniz, S. Y. AlQaradawi, J. W. Choi, A. Coskun, *ACS Nano* **2025**, *9*, 11317.
- [54] X. Wan, C. Kang, T. Mu, J. Zhu, P. Zuo, C. Du, G. Yin, *ACS Energy Lett.* **2022**, *7*, 3572.
- [55] Z. Zhao, J. Han, F. Chen, J. Xiao, Y. Zhao, Y. Zhang, D. Kong, Z. Weng, S. Wu, Q.-H. Yang, *Adv. Energy Mater.* **2022**, *12*, 2103565.

- [56] Y. Wang, H. Xu, X. Chen, H. Jin, J. Wang, *Energy Storage Mater.* **2021**, *38*, 121.
- [57] W. Jang, S. Kim, Y. Kang, T. Yim, T.-H. Kim, *Chem Eng J.* **2023**, *469*, 143949.
- [58] J. H. Hwang, E. Kim, E. Y. Lim, W. Lee, J. O. Kim, I. Choi, Y. S. Kim, D. G. Kim, J. H. Lee, J. C. Lee, *Adv. Sci.* **2023**, *10*, 2302144.
- [59] D. Jeong, J. Yook, D. S. Kwon, J. Shim, J. C. Lee, *Adv. Sci.* **2023**, *10*, 2302027.
- [60] G. Smolyakov, S. Pruvost, L. Cardoso, B. Alonso, E. Belamie, J. Duchet-Rumeau, *Carbohydr. Polym.* **2016**, *151*, 373.
- [61] Y. M. Y. Zhao, L. B. Li, H. Yang, S. B. Fan, S. Li, H. Tong, *Energy Storage Mater.* **2024**, *65*, 103126.
- [62] Z. Li, W. Tang, Y. Yang, G. Lai, Z. Lin, H. Xiao, J. Qiu, X. Wei, S. Wu, Z. Lin, *Adv. Funct. Mater.* **2022**, *32*, 2206615.
- [63] Z. Li, G. Wu, Y. Yang, X. Z. Wan, L. Yan, S. Wu, M. Ling, C. Liang, K. N. Hui, Z. Lin, *Adv. Energy Mater.* **2022**, *12*, 2201197.

Manuscript received: June 19, 2025

Revised manuscript received: August 6, 2025

Version of record online: